energies

MDPI

Article

Microgrid Assisted Design for Remote Areas

Guodong Liu [1,*], Zhi Li [1], Yaosuo Xue [1] and Kevin Tomsovic [2]

[1] Grid Components & Control Group, Oak Ridge National Laboratory, Oak Ridge, TN 37831, USA; lizhi@tsinghua-eiri.org (Z.L.); xuey@ornl.gov (Y.X.)
[2] Department of Electrical Engineering and Computer Science, The University of Tennessee, Knoxville, TN 37996, USA; tomsovic@utk.edu
* Correspondence: liug@ornl.gov; Tel.: +1-865-241-9732

Abstract: In this work, we present a three-stage multiobjective mixed-integer linear programming (MILP) for the optimal expansion planning and operation of isolated multienergy microgrids in remote areas. By selecting the optimal distributed generators (DGs) and energy storage systems (ESSs) mix selection, siting, sizing, and scheduling in the remote microgrid, the proposed model is targeted to minimize the annualized total cost of microgrids while enhancing the performance of the system, i.e., minimizing the voltage deviations and line power loss. To represent the electricity and heat flow between generation resources and various electrical, heating, and cooling loads in the isolated microgrid, linearized power flow, and heat flow constraints are employed in the proposed optimization model. The available capacity of DGs and ESSs are modeled as discrete constants instead of continuous variables for practical purpose. Numerical simulation results on a remote microgrid consisting of DGs, ESSs, and various loads validate the proposed method.

Keywords: microgrid; planning and operation; siting and sizing; mixed-integer linear programming (MILP)

check for updates

Citation: Liu, G.; Li, Z.; Xue, Y.; Tomsovic, K. Microgrid Assisted Design for Remote Areas. *Energies* **2022**, *15*, 3725. https://doi.org/10.3390/en15103725

Academic Editor: Andrea Bonfiglio

Received: 26 April 2022
Accepted: 17 May 2022
Published: 19 May 2022

Publisher's Note: MDPI stays neutral with regard to jurisdictional claims in published maps and institutional affiliations.

Copyright: © 2022 by the authors. Licensee MDPI, Basel, Switzerland. This article is an open access article distributed under the terms and conditions of the Creative Commons Attribution (CC BY) license (https://creativecommons.org/licenses/by/4.0/).

1. Introduction

A microgrid is a low-voltage energy system with distributed generators (DGs) and energy storage systems (ESSs) that are colocated with electrical and thermal loads. It is usually grid-connected through the Point of Common Coupling (PCC) but could automatically transform from grid-connected operation into islanded operation, in which a microgrid can continue to provide energy supply to its customers without any interruption in case of utility grid failures [1]. By virtue of its defining characteristics, microgrids introduce many unique opportunities, including improving the energy efficiency and reliability, facilitating renewable generation integration, reducing carbon emissions, delaying investment in distribution grid upgrades, and providing ancillary services, e.g., voltage and frequency regulation [2–5]. For these benefits, the number of microgrids deployed by utilities and customers has been growing rapidly in the last several years [6].

The remote segment (rural, remote, and islanded communities) has been leading the ever-increasing microgrid market, claiming the largest segment of overall microgrids worldwide with a share of 36% of the total market according to data released in a 2020 study [7]. The driving force of the prosperity of remote microgrids comes from different aspects of the market. Compared with traditional construction/upgrades of electrical network infrastructures requiring high investment and long commissioning timelines, deployment of microgrids is becoming favorable because of the increasingly lower cost of DGs and ESSs, no additional transmission/distribution line corridor needs, shorter construction cycles, and the ease of extending and upgrading. Microgrids enable an option for achieving cost-effective and reliable electricity supply for remote communities in a clean and sustainable way. Nevertheless, there are still challenges standing in almost every stage

of the microgrid adoption process, such as complexity to determine a site-specific optimal microgrid design that meets both economic and operational constraints.

There have been many existing literatures on optimization methods and algorithms for microgrid planning problem [8,9]. Generally, the microgrid planning problem could be formulated as a two-stage optimization, where the sizing and siting of DGs and ESSs are decided in the first-stage and the economic dispatch of installed DGs and ESSs are performed in the second-stage. In [10], wind turbine, diesel generator, and ESSs are optimally-sized for a remote microgrid. The objective is minimizing the energy cost and emissions. The problem is formulated as mixed-integer linear programming (MILP). Due to the fact that the power generation of renewable energy resources are highly variable, two-stage stochastic optimization models are more commonly proposed to take into account uncertainty of renewable generation, load variation and outages of DGs, etc., [11–13]. In [14], the design of microgrids is formulated as two-stage stochastic programming. The stochastic two-stage model is extended to minimize risk in the investment by modifying the objective function as Markovitz (mean-variance) objective function in [15]. The stochastic microgrid expansion planning problem is extended to consider the participation of microgrids in electricity markets in [16,17]. Considering the stochastic grid disturbances, renewable generation, and component outages, two-stage stochastic MILP models are proposed to determine the optimal sizing of DGs and ESSs to meet the specified resilience/reliability goals in [18,19]. Nevertheless, the formulation of stochastic optimization needs probability distribution of renewable generation, which might be difficult to obtain in reality.

Robust optimization ignores the probability distribution of stochastic variables, and makes the decision only based on the upper and lower bounds of them. Thus, robust optimization has gained increasing popularity recently. In [20], the microgrid planning is formulated as a two-stage robust optimization and solved using the column and constraint generation (C&CG) algorithm. In [21], the optimal planning of provisional microgrids is defined and formulated as robust optimization. In [22], renewable generation and load are modeled through Wasserstein metric-based ambiguity sets. Then, the optimal planning of microgrids is formulated as a data-driven two-stage robust optimization. Combining stochastic optimization and robust optimization, a hybrid stochastic-robust optimization model is proposed for resilient microgrid planning in [23]. Note that two-stage robust optimization models require the inner-level optimization to be linear, so that it could be equivalently transformed into its dual problem, then C&CG or benders' decomposition algorithms could be utilized to solve the optimization efficiently. As a result, the commitment status and minimum output of dispatchable DGs have been ignored.

Some of these classic stochastic and robust methods have been implemented by software tools. HOMER creates a list of feasible configurations based on alternative time-series simulations, then selects the best plan economically and environmentally [24]. DER-CAM software is focusing on building microgrid technology selection and operation [25]. Besides classic mathematical programming methods, metaheuristic methods have also been widely used for solving the microgrid planning and expansion problem due to the capability to deal with non-convex constraints and objectives. These metaheuristic methods includes genetic algorithm (GA) [26,27], particle swarm optimization (PSO) [28,29], simulated annealing (SA) method [30,31], harmony search algorithm (HSA) [32], grasshopper optimization algorithm (GOA) [33], grey wolf algorithm (GWA) [34], whale optimization algorithm (WOA) [35], etc. Nevertheless, the optimality of solution cannot be guaranteed by metaheuristic methods.

Considering electricity, heating, and cooling demand, a multiobjective optimization is proposed for the optimal expansion planning and operation of isolated microgrids. The proposed model minimize the annualized investment and operation costs of microgrids; at the same time, it enhances the performance of the system, i.e., minimizing the voltage deviations and line power loss by selecting the optimal DGs and ESSs mix selection, siting, sizing, and scheduling in remote microgrids. Considering the commitment status and minimum output of dispatchable DGs, especially legacy diesel generation sets, the proposed

microgrid expansion planning model is formulated as three-stage MILP. Linearized power flow and heat flow equations are employed in the proposed optimization as constraints to explicitly model the energy flow. The main contributions of this paper are as follows:

- A three-stage MILP is proposed for optimal expansion planning and operation of isolated multienergy microgrids considering legacy DGs and ESSs.
- For practical purpose, the available capacity of DGs (except PV) and ESSs is modeled as discrete constants instead of continuous variables. In addition, the commitment status and minimum output of dispatchable DGs are explicitly modeled.
- To represent the electricity and heat flow between generation resources and various electrical, heating and cooling loads in the isolated microgrid, linearized power flow and heat flow constraints are employed in the proposed optimization model.

This paper is structured as follows: microgrid components and the proposed three-stage MILP for optimal expansion planning and operation of isolated multienergy microgrids are presented in Section 2. Numerical simulation results and analysis are presented in Section 3. Conclusions are drawn in Section 4.

2. Mathematical Formulations

2.1. Microgrid Components

Traditionally, microgrids in remote areas are designed based on diesel generators, which are subject to expensive cost, low efficiency, heavy emissions, and huge fluctuations of petroleum price. Currently, DGs, e.g., gas turbines, fuel cells, and their combined heat and power (CHP) applications, are more attractive options due to their increasing lower cost, little pollutants, and less maintenance, etc. Renewable DGs, e.g., wind turbine and PV, are even gaining unprecedented popularity due to the unique characteristic of little to no greenhouse gas emissions. However, wind and PV generation are affected by the changing weather conditions. As a result, they could only be forecasted with limited accuracy. The hour-ahead forecast error of wind power output could be achieved below 10% [36,37]. As for PV power, it is even more volatile due to changing cloud coverage and ambient temperature [38,39]. To mitigate these intermittency and uncertainties, ESSs are usually equipped on-site.

In this paper, it is assumed that the available options of invested technologies include gas turbine, gas turbine CHP, fuel cell, fuel cell CHP, PV, and ESS. For each technology, there are a variety of selections with different characteristics (such as capacity, size, efficiency, etc.). PV capacity is taken as continuous variables limited by available spaces. For gas turbine, gas turbine CHP, fuel cell, fuel cell CHP, and ESS, there are only a limited number of capacities available based on existing commercial products. Thus, a binary variable is created for each candidate component with specific capacity. Without loss of generality, wind turbines are not taken as available investment options in this work due to concerns existing over noise pollution and threats to the wildlife. In addition, it is assumed that the electricity and heating distribution network has already been installed, thus only planning of DGs and ESSs is considered in this work.

2.2. Objective Function

The problem of optimal expansion planning and operation of isolated multienergy microgrids in remote areas is formulated as a three-stage MILP model. By selecting the optimal DGs and ESSs mix selection, siting, sizing, and scheduling in the remote microgrid, the proposed model is targeted to minimize the annualized investment and operation costs of microgrids; at the same time, it enhances the performance of the system, i.e., minimizing the voltage deviations and line power loss, as shown in (1). The multiple objectives are integrated into a single objective function by weighted summation. W_C, W_V and W_L are weighting factors of system investment and operation cost, voltage deviations, and line power losses, respectively. For simplicity, W_C, W_V and W_L are all set to be 1 in this paper. An analytical hierarchy process (AHP) was proposed to help setting weighting factors based on pairwise comparison of the importance of any two objectives [40]. The basic idea

of this work is to determine whether by adding certain new DGs and ESSs in an existing microgrid, we could reduce the annualized overall cost of the microgrid, i.e., improve the energy economy.

$$\min \quad \mathrm{W_C}\left(IC + OC + \mathrm{OC^{EX}}\right) + \mathrm{W_V}VD + \mathrm{W_L}LOSS \tag{1}$$

The annualized investment cost is shown in (2), which includes PV, gas turbine, gas turbine CHP, fuel cell, fuel cell CHP, and ESS. The PV capacity are modeled as continuous variables, while other DGs are modeled with binary variables. Take fuel cell, for example, U_{nji}^{FC} is a binary variable indicating whether fuel cell i of size selection j is invested at bus n or not. The term $\frac{r(1+r)^{l_j^{FC}}}{(1+r)^{l_j^{FC}}-1}$ is an annuity factor that equally distributes the overall investment cost into l_j^{FC} years, where l_j^{FC} is the lifetime of the fuel cell.

$$\begin{aligned}
\mathrm{IC} \;=\; & \sum_{n=1}^{NN}\sum_{i=1}^{NPV}\frac{r(1+r)^{l_i^{PV}}}{(1+r)^{l_i^{PV}}-1}C_i^{PV}Cap_{ni}^{PV} \\
& + \sum_{n=1}^{NN}\sum_{j=1}^{NFC}\sum_{i=1}^{NFC_j}\frac{r(1+r)^{l_j^{FC}}}{(1+r)^{l_j^{FC}}-1}C_j^{FC}Cap_j^{FC}U_{nji}^{FC} \\
& + \sum_{n=1}^{NN}\sum_{j=1}^{NFCC}\sum_{i=1}^{NFCC_j}\frac{r(1+r)^{l_j^{FCC}}}{(1+r)^{l_j^{FCC}}-1}C_j^{FCC}Cap_j^{FCC}U_{nji}^{FCC} \\
& + \sum_{n=1}^{NN}\sum_{j=1}^{NGT}\sum_{i=1}^{NGT_j}\frac{r(1+r)^{l_j^{GT}}}{(1+r)^{l_j^{GT}}-1}C_j^{GT}Cap_j^{GT}U_{nji}^{GT} \\
& + \sum_{n=1}^{NN}\sum_{j=1}^{NGTC}\sum_{i=1}^{NGTC_j}\frac{r(1+r)^{l_j^{GTC}}}{(1+r)^{l_j^{GTC}}-1}C_j^{GTC}Cap_j^{GTC}U_{nji}^{GTC} \\
& + \sum_{n=1}^{NN}\sum_{j=1}^{NBT}\sum_{i=1}^{NBT_j}+\frac{r(1+r)^{l_j^{BT}}}{(1+r)^{l_j^{BT}}-1}C_j^{BT}U_{nji}^{BT}
\end{aligned} \tag{2}$$

The annualized operating cost includes that of new invested DGs and ESS as shown in (4), as well as legacy DGs and ESSs as shown in (5). For new invested DGs and ESSs, the operating cost includes fixed O&M cost, fuel cost of DGs, and degradation cost of ESSs as in (4). For legacy DGs and ESSs, the operating cost includes fuel cost of DGs, degradation cost of ESSs, and cost of natural gas burned for direct heating as in (5).

Note that the operating costs of DGs are assumed piecewise linear, which has been widely used in existing literatures [41,42], commercial microgrid planning and operation tools [43], and real electricity markets [44,45]. As to ESSs, detailed ESS degradation is a complex process affected by many factors (e.g., temperature, depth of discharge, charging/discharging rate, type and manufacture of ESS, etc.) [46]. Nevertheless, the ESS degradation cost can be approximately formulated as a linear function of the charged and discharged energy [47,48].

$$\begin{aligned}
\mathrm{OC} \;=\; & \sum_{n=1}^{NN}\sum_{i=1}^{NPV}COM_i^{PV}Cap_{ni}^{PV} \\
& + \sum_{n=1}^{NN}\sum_{j=1}^{NFC}\sum_{i=1}^{NFC_j}\left\{COM_j^{FC}Cap_j^{FC}U_{nji}^{FC} + \sum_{t=1}^{NT}\left[\sum_{m=1}^{NI}\lambda_j^{FC}(m)p_{njit}^{FC}(m) + \kappa_j^{FC}u_{njit}^{FC}\right]\right\} \\
& + \sum_{n=1}^{NN}\sum_{j=1}^{NFCC}\sum_{i=1}^{NFCC_j}\left\{COM_j^{FCC}Cap_j^{FCC}U_{nji}^{FCC} + \sum_{t=1}^{NT}\left[\sum_{m=1}^{NI}\lambda_j^{FCC}(m)p_{njit}^{FCC}(m) + \kappa_j^{FCC}u_{njit}^{FCC}\right]\right\}
\end{aligned}$$

$$+\sum_{n=1}^{NN}\sum_{j=1}^{NGT}\sum_{i=1}^{NGT_j}\left\{COM_j^{GT}Cap_j^{GT}U_{nji}^{GT}+\sum_{t=1}^{NT}\left[\sum_{m=1}^{NI}\lambda_j^{GT}(m)p_{njit}^{GT}(m)+\kappa_j^{GT}u_{njit}^{GT}\right]\right\} \tag{3}$$
$$+\sum_{n=1}^{NN}\sum_{j=1}^{NGTC}\sum_{i=1}^{NGTC_j}\left\{COM_j^{GTC}Cap_j^{GTC}U_{nji}^{GTC}+\sum_{t=1}^{NT}\left[\sum_{m=1}^{NI}\lambda_j^{GTC}(m)p_{njit}^{GTC}(m)+\kappa_j^{GTC}u_{njit}^{GTC}\right]\right\}$$
$$+\sum_{n=1}^{NN}\sum_{j=1}^{NBT}\sum_{i=1}^{NBT_j}\left[COM_j^{BT}U_{nji}^{BT}+\sum_{t=1}^{NT}\left(\lambda_j^{ch}p_{njit}^{ch}+\lambda_j^{dch}p_{njit}^{dch}\right)\right]$$

$$\begin{aligned}\mathrm{OC^{EX}} = &\sum_{i=1}^{NDG_{EX}}\sum_{t=1}^{NT}\left[\sum_{m=1}^{NI}\lambda_i^{DG_{EX}}(m)p_{it}^{DG_{EX}}(m)+\kappa_i^{DG_{EX}}u_{it}^{DG_{EX}}\right]\\ &+\sum_{i=1}^{NFC_{EX}}\sum_{t=1}^{NT}\left[\sum_{m=1}^{NI}\lambda_i^{FC_{EX}}(m)p_{it}^{FC_{EX}}(m)+\kappa_i^{FC_{EX}}u_{it}^{FC_{EX}}\right]\\ &+\sum_{i=1}^{NFCC_{EX}}\sum_{t=1}^{NT}\left[\sum_{m=1}^{NI}\lambda_i^{FCC_{EX}}(m)p_{it}^{FCC_{EX}}(m)+\kappa_i^{FCC_{EX}}u_{it}^{FCC_{EX}}\right]\\ &+\sum_{i=1}^{NGT_{EX}}\sum_{t=1}^{NT}\left[\sum_{m=1}^{NI}\lambda_i^{GT_{EX}}(m)p_{it}^{GT_{EX}}(m)+\kappa_i^{GT_{EX}}u_{it}^{GT_{EX}}\right]\\ &+\sum_{i=1}^{NGTC_{EX}}\sum_{t=1}^{NT}\left[\sum_{m=1}^{NI}\lambda_i^{GTC}(m)p_{it}^{GTC_{EX}}(m)+\kappa_i^{GTC_{EX}}u_{it}^{GTC_{EX}}\right]\\ &+\sum_{i=1}^{NBT_{EX}}\sum_{t=1}^{NT}\left(\lambda_i^{ch_{EX}}p_{it}^{ch_{EX}}+\lambda_i^{dch_{EX}}p_{it}^{dch_{EX}}\right)\\ &+\sum_{n=1}^{NN}\sum_{t=1}^{NT}\lambda_{nt}^{G}G_{nt}\end{aligned} \tag{4}$$

The system total voltage deviations and line power losses are shown in (5) and (6), which will be linearized in the following subsection.

$$VD = \sum_{t=1}^{N_T}\sum_{n=1}^{N_N}V_{nt}^2-(V_{\mathrm{thr}}^{\max})^2:\ (V_{nt}>V_{\mathrm{thr}}^{\max})+\sum_{t=1}^{N_T}\sum_{n=1}^{N_N}\left(V_{\mathrm{thr}}^{\min}\right)^2-V_{nt}^2:\ (V_{nt}<V_{\mathrm{thr}}^{\min}) \tag{5}$$

$$LOSS = \sum_{f=1}^{NC}\sum_{t=1}^{NT}r_f\left(P_{ft}^2+Q_{ft}^2\right) \tag{6}$$

The proposed model for optimal expansion planning and operation of isolated multi-energy microgrids is a three-stage MILP model. In the first stage, the investment decisions of distributed generators (DGs) and energy storage systems (ESSs) are determined through optimizing the binary variables U_{nji}^{FC}, U_{nji}^{FCC}, U_{nji}^{GT}, U_{nji}^{GTC}, U_{nji}^{BT}, and continuous variable Cap_{ni}^{PV}. Note these variables are associated with each bus n, each selection j for a technology and each candidate unit number i for technology selection j, i.e., these first-stage variables determine the DGs and ESSs mix selection, siting, and sizing. In the second stage, the commitment status of dispatchable DGs and charging/discharging status of ESSs are solved. In the third stage, the dispatching decisions of DGs and ESSs are decided, i.e., the scheduling of new invested and existing DGs and ESSs are determined through optimizing the second-stage and third-stage variables.

2.3. Constraints

The objective is subject to constraints associated with each component and other system operation limits, such as power balance, heating balance, cooling balance, voltage limits, and power/heat flow limits.

2.3.1. PV Constraints

$$\sum_{i=1}^{NPV} Cap_{ni}^{PV} S_i^{PV} \leq \Delta_n^{max} \quad \forall n \tag{7}$$

$$P_{nit}^{PV} = Cap_{ni}^{PV} \frac{G_t}{G_{STC}} [1 + k(T_c - T_r)] \tag{8}$$

The maximum invested PV capacity is limited by the available area at each bus as in (7). A maximum power point tracker is assumed, and the maximum power output of PV is represented as a linear function of invested PV capacity as in (8) [49].

2.3.2. Fuel Cell Constraints

$$P_{njit}^{FC} = \sum_{m=1}^{NI} p_{njit}^{FC}(m) + u_{njit}^{FC} P_j^{FC,min} \quad \forall n, \forall j, \forall i, \forall t \tag{9}$$

$$0 \leq p_{njit}^{FC}(m) \leq p_{njit}^{FC,max}(m) \quad \forall n, \forall j, \forall i, \forall t, \forall m \tag{10}$$

$$u_{njit}^{FC} \leq U_{nji}^{FC} \quad \forall n, \forall j, \forall i, \forall t \tag{11}$$

$$P_j^{FC,min} u_{njit}^{FC} \leq P_{njit}^{FC} \leq P_j^{FC,max} u_{njit}^{FC} \quad \forall n, \forall j, \forall i, \forall t \tag{12}$$

$$-\tan\left(\cos^{-1}\left(PF_j^{FC,min}\right)\right) P_{njit}^{FC} \leq Q_{njit}^{FC} \leq tan\left(\cos^{-1}\left(PF_j^{FC,max}\right)\right) P_{njit}^{FC} \tag{13}$$

$$\left(P_{njit}^{FC}\right)^2 + \left(Q_{njit}^{FC}\right)^2 \leq \left(S_j^{FC}\right)^2 \quad \forall n, \forall j, \forall i, \forall t \tag{14}$$

The fuel cost of fuel cell is approximated by blocks through constraints (9) and (10). Constraint (11) enforces the output of fuel cell to be zero if not invested. The minimum and maximum output of fuel cell is enforced by (12). The power factor and capacity limit is ensured by (13) and (14).

2.3.3. Fuel Cell CHP Constraints

$$P_{njit}^{FCC} = \sum_{m=1}^{NI} p_{njit}^{FCC}(m) + u_{njit}^{FCC} P_j^{FCC,min} \quad \forall n, \forall j, \forall i, \forall t \tag{15}$$

$$0 \leq p_{njit}^{FCC}(m) \leq p_{njit}^{FCC,max}(m) \quad \forall n, \forall j, \forall i, \forall t, \forall m \tag{16}$$

$$u_{njit}^{FCC} \leq U_{nji}^{FCC} \quad \forall n, \forall j, \forall i, \forall t \tag{17}$$

$$P_j^{FCC,min} u_{njit}^{FCC} \leq P_{njit}^{FCC} \leq P_j^{FCC,max} u_{njit}^{FCC} \quad \forall n, \forall j, \forall i, \forall t \tag{18}$$

$$-\tan\left(\cos^{-1}\left(PF_j^{FCC,min}\right)\right) P_{njit}^{FCC} \leq Q_{njit}^{FCC} \leq tan\left(\cos^{-1}\left(PF_j^{FCC,max}\right)\right) P_{njit}^{FCC} \tag{19}$$

$$\left(P_{njit}^{FCC}\right)^2 + \left(Q_{njit}^{FCC}\right)^2 \leq \left(S_j^{FCC}\right)^2 \quad \forall n, \forall j, \forall i, \forall t \tag{20}$$

$$0 \leq H_{njit}^{FCC} \leq HPR_j^{FCC} P_{njit}^{FCC} \quad \forall n, \forall j, \forall i, \forall t \tag{21}$$

The fuel cost of fuel cell CHP is approximated by blocks through constraints (15) and (16). Constraint (17) enforces the output of fuel cell CHP to be zero if not invested. The minimum and maximum output of fuel cell CHP is enforced by (18). The power factor and capacity limit are ensured by (19) and (20). The heating output of fuel cell CHP is limited by the heating to power ratio (HPR) as in (21).

2.3.4. Gas Turbine Constraints

$$P_{njit}^{GT} = \sum_{m=1}^{NI} p_{njit}^{GT}(m) + u_{njit}^{GT} P_j^{GT,min} \quad \forall n, \forall j, \forall i, \forall t \tag{22}$$

$$0 \le p_{njit}^{GT}(m) \le p_{njit}^{GT,max}(m) \quad \forall n, \forall j, \forall i, \forall t, \forall m \tag{23}$$

$$u_{njit}^{GT} \le U_{nji}^{GT} \quad \forall n, \forall j, \forall i, \forall t \tag{24}$$

$$P_j^{GT,min} u_{njit}^{GT} \le P_{njit}^{GT} \le P_j^{GT,max} u_{njit}^{GT} \quad \forall n, \forall j, \forall i, \forall t \tag{25}$$

$$-\tan\left(\cos^{-1}\left(PF_j^{FC,min}\right)\right) P_{njit}^{GT} \le Q_{njit}^{GT} \le tan\left(\cos^{-1}\left(PF_j^{GT,max}\right)\right) P_{njit}^{GT} \tag{26}$$

$$\left(P_{njit}^{GT}\right)^2 + \left(Q_{njit}^{GT}\right)^2 \le \left(S_j^{GT}\right)^2 \quad \forall n, \forall j, \forall i, \forall t \tag{27}$$

The fuel cost of gas turbine is approximated by blocks through constraints (22) and (23). Constraint (24) enforces the output of gas turbine to be zero if not invested. The minimum and maximum output of gas turbine is enforced by (25). The power factor and capacity limit is ensured by (26) and (27).

2.3.5. Gas Turbine CHP Constraints

$$P_{njit}^{GTC} = \sum_{m=1}^{NI} p_{njit}^{GTC}(m) + u_{njit}^{GTC} P_j^{GTC,min} \quad \forall n, \forall j, \forall i, \forall t \tag{28}$$

$$0 \le p_{njit}^{GTC}(m) \le p_{njit}^{GTC,max}(m) \quad \forall n, \forall j, \forall i, \forall t, \forall m \tag{29}$$

$$u_{njit}^{GTC} \le U_{nji}^{GTC} \quad \forall n, \forall j, \forall i, \forall t \tag{30}$$

$$P_j^{GTC,min} u_{njit}^{GTC} \le P_{njit}^{GTC} \le P_j^{GTC,max} u_{njit}^{GTC} \quad \forall n, \forall j, \forall i, \forall t \tag{31}$$

$$-\tan\left(\cos^{-1}\left(PF_j^{GTC,min}\right)\right) P_{njit}^{GTC} \le Q_{njit}^{GTC} \le tan\left(\cos^{-1}\left(PF_j^{GTC,max}\right)\right) P_{njit}^{GTC} \tag{32}$$

$$\left(P_{njit}^{GTC}\right)^2 + \left(Q_{njit}^{GTC}\right)^2 \le \left(S_j^{GTC}\right)^2 \quad \forall n, \forall j, \forall i, \forall t \tag{33}$$

$$0 \le H_{njit}^{GTC} \le HPR_j^{GTC} P_{njit}^{GTC} \quad \forall n, \forall j, \forall i, \forall t \tag{34}$$

The fuel cost of fuel cell CHP is approximated by blocks through constraints (28) and (29). Constraint (30) enforces the output of fuel cell CHP to be zero if not invested. The minimum and maximum output of fuel cell CHP is enforced by (31). The power factor and capacity limit is ensured by (32) and (33). The heating output of gas turbine CHP is limited by the heating to power ratio (HPR) as in (34).

2.3.6. ESS Constraints

$$0 \le P_{njit}^{ch} \le P_j^{ch,max} u_{njit}^{\mathrm{C}} \quad \forall n, \forall j, \forall i, \forall t \tag{35}$$

$$0 \le P_{njit}^{dch} \le P_j^{dch,max} u_{njit}^{D} \quad \forall n, \forall j, \forall i, \forall t \tag{36}$$

$$u_{njit}^{\mathrm{C}} + u_{njit}^{\mathrm{D}} \le 1 \quad \forall n, \forall j, \forall i, \forall t \tag{37}$$

$$u_{njit}^{\mathrm{C}} \le U_{nji}^{BT} \quad \forall n, \forall j, \forall i, \forall t \tag{38}$$

$$u_{njit}^{\mathrm{D}} \le U_{nji}^{BT} \quad \forall n, \forall j, \forall i, \forall t \tag{39}$$

$$SOC_{njit}^{BT} = SOC_{nji,t-1}^{BT} + P_{njit}^{ch} \eta_j^{\mathrm{C}} \triangle t - P_{njit}^{dch} \frac{1}{\eta_j^{\mathrm{C}}} \triangle t \quad \forall n, \forall j, \forall i, \forall t \tag{40}$$

$$SOC_j^{\mathrm{BT,min}} \leq SOC_{njit} \leq SOC_j^{BT,\max} \quad \forall n, \forall j, \forall i, \forall t \tag{41}$$

$$\begin{aligned} -\tan\left(\cos^{-1}\left(PF_j^{BT,C,min}\right)\right)P_{njit}^{ch} \quad &\leq \quad Q_{njit}^{BT} \leq \tan\left(\cos^{-1}\left(PF_j^{BT,C,max}\right)\right)P_{njit}^{ch} \\ &if \quad : P_{njit}^{ch} > 0 \,\forall n, \forall j, \forall i, \forall t \end{aligned} \tag{42}$$

$$\begin{aligned} -\tan\left(\cos^{-1}\left(PF_j^{BT,D,min}\right)\right)P_{njit}^{dch} \quad &\leq \quad Q_{njit}^{BT} \leq \tan\left(\cos^{-1}\left(PF_j^{BT,D,max}\right)\right)P_{njit}^{dch} \\ &if \quad : P_{njit}^{dch} > 0 \,\forall n, \forall j, \forall i, \forall t \end{aligned} \tag{43}$$

$$\left(P_{njit}^{dch} - P_{njit}^{ch}\right)^2 + \left(Q_{njit}^{BT}\right)^2 \leq \left(S_j^{BT}\right)^2 \quad \forall n, \forall j, \forall i, \forall t \tag{44}$$

The maximum charging/discharging power of an ESS is constrained by (35) and (36). These two states are mutually exclusive; this is ensured by (37). The ESS cannot charge or discharge any power when it is not invested. This constraint is represented by (38) and (39).The minimum and maximum state of charge (SOC) are specified in (40) and (41). The power factor limits of an ESS are represented in (42) and (43). The capacity of an ESS is enforced by (44). The logical terms in constraints (42) and (43) are reformulated into mixed-integer linear (MIL) form, as (45)–(48).

$$-S_j^{BT}u_{njit}^{\mathrm{D}} - \tan\left(\cos^{-1}\left(PF_j^{BT,C,min}\right)\right)P_{njit}^{ch} \leq Q_{njit}^{BT} \forall n, \forall j, \forall i, \forall t \tag{45}$$

$$Q_{njit}^{BT} \leq \tan\left(\cos^{-1}\left(PF_j^{BT,C,max}\right)\right)P_{njit}^{ch} + S_j^{BT}u_{njit}^{\mathrm{D}} \forall n, \forall j, \forall i, \forall t \tag{46}$$

$$-S_j^{BT}u_{njit}^{\mathrm{C}} - \tan\left(\cos^{-1}\left(PF_j^{BT,D,min}\right)\right)P_{njit}^{dch} \leq Q_{njit}^{BT} \forall n, \forall j, \forall i, \forall t \tag{47}$$

$$Q_{njit}^{BT} \leq \tan\left(\cos^{-1}\left(PF_j^{BT,D,max}\right)\right)P_{njit}^{dch} + S_j^{BT}u_{njit}^{\mathrm{C}} \forall n, \forall j, \forall i, \forall t \tag{48}$$

2.3.7. Network Constraints

Equations (49)–(53) are the linear DistFlow model (LinDistFlow), which was first proposed in [50]. The LinDistFlow model is one of the most widely used linear power flow models for distribution system analysis due to its ability to yield accurate voltage magnitude estimations under radial topology and high r/x ratio [51–53]. For the accuracy of the LinDistFlow model, we refer readers to [54], which validated the LinDistFlow model on different IEEE test feeders. The bus voltage drop is specified in (49). The real and reactive power are balanced across the network, which are ensured by (50) and (51), where A^{Inc} is the nodal incidence matrix of the electricity distribution network. The bus voltages are limited by (52). The feeder capacity is enforced by (53). Note that the square of nodal voltages in (49) and (52) are directly taken as variables. Thus, these two constraints are linear.

$$V_{nt}^2 = V_{n+1,t}^2 + 2\left(r_f P_{ft} + x_f Q_{ft}\right) \quad \forall f, \forall t \tag{49}$$

$$\begin{aligned} A^{\mathrm{Inc}}\mathbf{P_f} \quad = \quad & A_{PV}^{\mathrm{Inc}}\mathbf{P^{PV}} + A_{FC}^{\mathrm{Inc}}\mathbf{P^{FC}} + A_{FCC}^{\mathrm{Inc}}\mathbf{P^{FCC}} + A_{GT}^{\mathrm{Inc}}\mathbf{P^{GT}} \\ & + A_{GTC}^{\mathrm{Inc}}\mathbf{P^{GTC}} + A_{BT}^{\mathrm{Inc}}\left(\mathbf{P^{dch}} - \mathbf{P^{ch}}\right) + A_{PV_{EX}}^{\mathrm{Inc}}\mathbf{P^{PV_{EX}}} \\ & + A_{DG_{EX}}^{\mathrm{Inc}}\mathbf{P^{DG_{EX}}} + A_{FC_{EX}}^{\mathrm{Inc}}\mathbf{P^{FC_{EX}}} + A_{FCC_{EX}}^{\mathrm{Inc}}\mathbf{P^{FCC_{EX}}} \\ & + A_{GT_{EX}}^{\mathrm{Inc}}\mathbf{P^{GT_{EX}}} + A_{GTC}^{\mathrm{Inc}}\mathbf{P^{GTC_{EX}}} + A_{BT_{EX}}^{\mathrm{Inc}}\left(\mathbf{P^{dch_{EX}}} - \mathbf{P^{ch_{EX}}}\right) \\ & - A_L^{\mathrm{Inc}}\left(\mathbf{P^L} + \mathbf{P^H} + \mathbf{P^C}\right) \end{aligned} \tag{50}$$

$$\begin{aligned} A^{\text{Inc}}\mathbf{Q_f} \;=\; & A^{\text{Inc}}_{FC}\mathbf{Q^{FC}} + A^{\text{Inc}}_{FCC}\mathbf{Q^{FCC}} + A^{\text{Inc}}_{GT}\mathbf{Q^{GT}} + A^{\text{Inc}}_{GTC}\mathbf{Q^{GTC}} \\ & + A^{\text{Inc}}_{BT}\mathbf{Q^{BT}} + A^{\text{Inc}}_{DG_{EX}}\mathbf{Q^{DG_{EX}}} + A^{\text{Inc}}_{FC_{EX}}\mathbf{Q^{FC_{EX}}} \\ & + A^{\text{Inc}}_{FCC_{EX}}\mathbf{Q^{FCC_{EX}}} + A^{\text{Inc}}_{GT_{EX}}\mathbf{Q^{GT_{EX}}} + A^{\text{Inc}}_{GTC}\mathbf{Q^{GTC_{EX}}} \\ & + A^{\text{Inc}}_{BT_{EX}}\mathbf{Q^{BT_{EX}}} - A^{\text{Inc}}_{L}\mathbf{Q^{L}} \end{aligned} \tag{51}$$

$$\left(V^{\min}\right)^2 \le V_{nt}^2 \le (V^{\max})^2 \quad \forall n, \forall t \tag{52}$$

$$P_{ft}^2 + Q_{ft}^2 \le S_f^2 \quad \forall f, \forall t \tag{53}$$

Similarly, the heating balances across the heating distribution network are represented by (54), where B^{Inc} is the nodal incidence matrix of the heating distribution network. The heating and cooling loads are satisfied by (55) and (56). For a system without heating distribution network, we simply need to enforce $\mathbf{H_f} = \mathbf{0}$.

$$\begin{aligned} B^{\text{Inc}}\mathbf{H_f} \;=\; & \left(B^{\text{Inc}}_{FCC}\mathbf{H^{FCC}} + B^{\text{Inc}}_{GTC}\mathbf{H^{GTC}} + B^{\text{Inc}}_{FCC_{EX}}\mathbf{H^{FCC_{EX}}} + B^{\text{Inc}}_{GTC}\mathbf{H^{GTC}}\right)\beta^R \\ & - B^{\text{Inc}}_{L}\mathbf{G}\beta^G - B^{\text{Inc}}_{L}\left(\mathbf{H^H} + \mathbf{H^C}\right) \end{aligned} \tag{54}$$

$$H_{nt}^H + \delta^H P_{nt}^H \ge L_{nt}^H \tag{55}$$

$$\gamma^C H_{nt}^C + \delta^C P_{nt}^C \ge L_{nt}^C \tag{56}$$

The energy flow diagram is shown in Figure 1. In particular, we consider the heating and cooling demand into the optimization model. The heating demand must be satisfied by electricity power heat pump or recovered heat from CHP and fuel burner. Meanwhile, the cooling demand must be satisfied by electricity power heat pump or absorption chiller, which utilizes recovered heat from CHP and fuel burner.

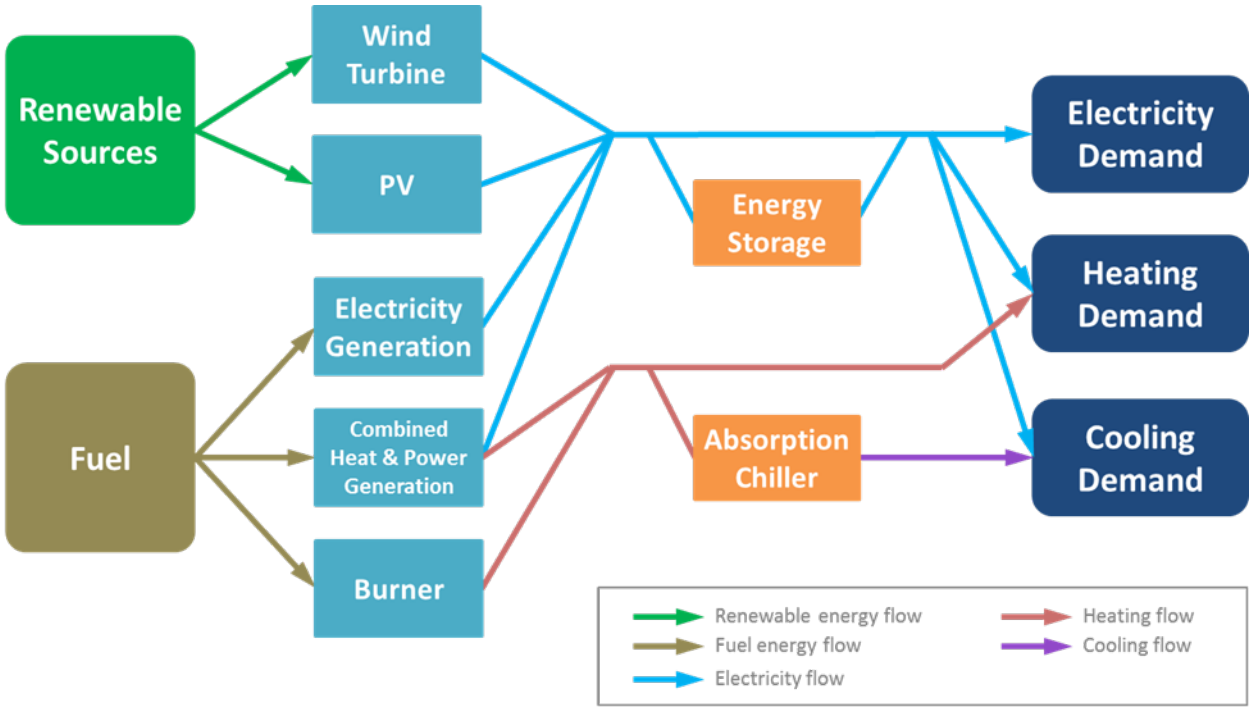

Figure 1. Energy flow diagram of remote multienergy microgrids.

2.3.8. Simplification and Linearization

To reformulate the proposed planning model for isolated multienergy microgrids in remote areas into MILP, all nonlinear terms in the objective function and constraints have to be reformulated or linearized into MIL form. In the objective function, the logic expression

of voltage deviation in (5) could be reformulated into linear format as (57)–(59), where X_{nt}^{V} is the absolute voltage deviation.

$$X_{nt}^{V} \geq V_{nt}^{2} - (V_{\text{thr}}^{\max})^{2} \quad \forall n, \forall t \tag{57}$$

$$X_{nt}^{V} \geq \left(V_{\text{thr}}^{\min}\right)^{2} - V_{nt}^{2} \quad \forall n, \forall t \tag{58}$$

$$X_{nt}^{V} \geq 0 \quad \forall n, \forall t \tag{59}$$

The quadratic terms in the total line losses in equation (6) can be estimated by piecewise linearization [55]. The same linearization can be performed for quadratic capacity constraints (14), (20), (27), (33), and (44).

Finally, all nonlinear constraints have been equivalently transformed into MIL form. As a result, the proposed microgrid planning model is now a MILP, which could be solved by open-source MILP solvers (e.g., Coin-OR CBC) or commercial MILP solvers efficiently.

A workflow diagram of the proposed optimal expansion planning and operation for isolated multienergy microgrids is shown in Figure 2. As can be seen, the economic characteristic, component characteristics, system data, and investment options are the input data. Based on these data, the problem of optimal expansion planning and operation of isolated multienergy microgrids is formulated as a three-stage MILP model considering both power flow and heat flow constraints. The formulated model is solved by commercial or free MILP solvers. Finally, the optimal design and corresponding results are obtained.

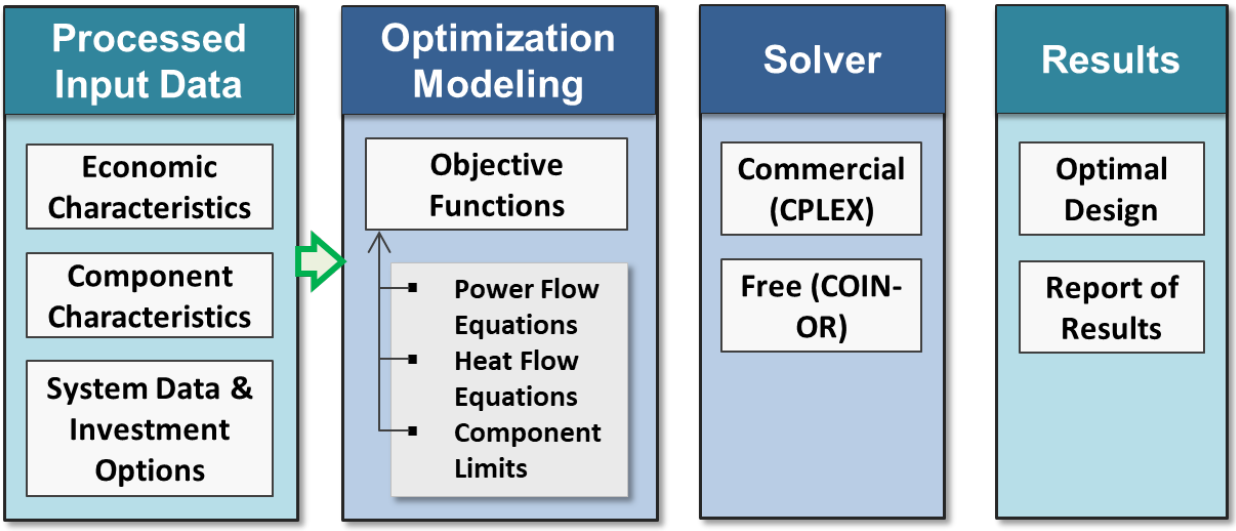

Figure 2. Workflow diagram of the proposed optimal expansion planning and operation for isolated multienergy microgrids.

3. Case Studies

3.1. Test System

The proposed model for microgrid expansion planning and operation was demonstrated using a modified Oak Ridge National Laboratory (ORNL) Distributed Energy Control and Communication (DECC) microgrid test system [56]. The test system includes 5 buses, 4 dispatchable DGs, 2 groups of PV panels, a battery, and 3 multienergy loads, as shown in Figure 3.

The parameters of dispatchable DGs can be found in [57]. The parameters of the existing battery are listed in Table 1.

Table 1. Existing Battery parameters.

Battery Type	Power Capacity (kW)	Energy Capacity (kWh)	SOC^{max} (%)	SOC^{min} (%)
Lithium-ion	50	100	95	25
Degradation Cost ($/kWh)	**Charging Efficiency (%)**	**Discharging Efficiency (%)**	**Initial SOC (%)**	**End SOC (%)**
0.02	0.95	0.95	50	50

The microgrid has 13.4 kW roof top PV installed on bus 1 and another 50 kW PV installed on bus 2. The measured 1-min solar irradiance and temperature of Oak Ridge, Tennessee area in 2015 is used [58]. To reduce the computational burden, each month is simplified as one day; thus, only 12 days are used and the operating costs are scaled to one year.

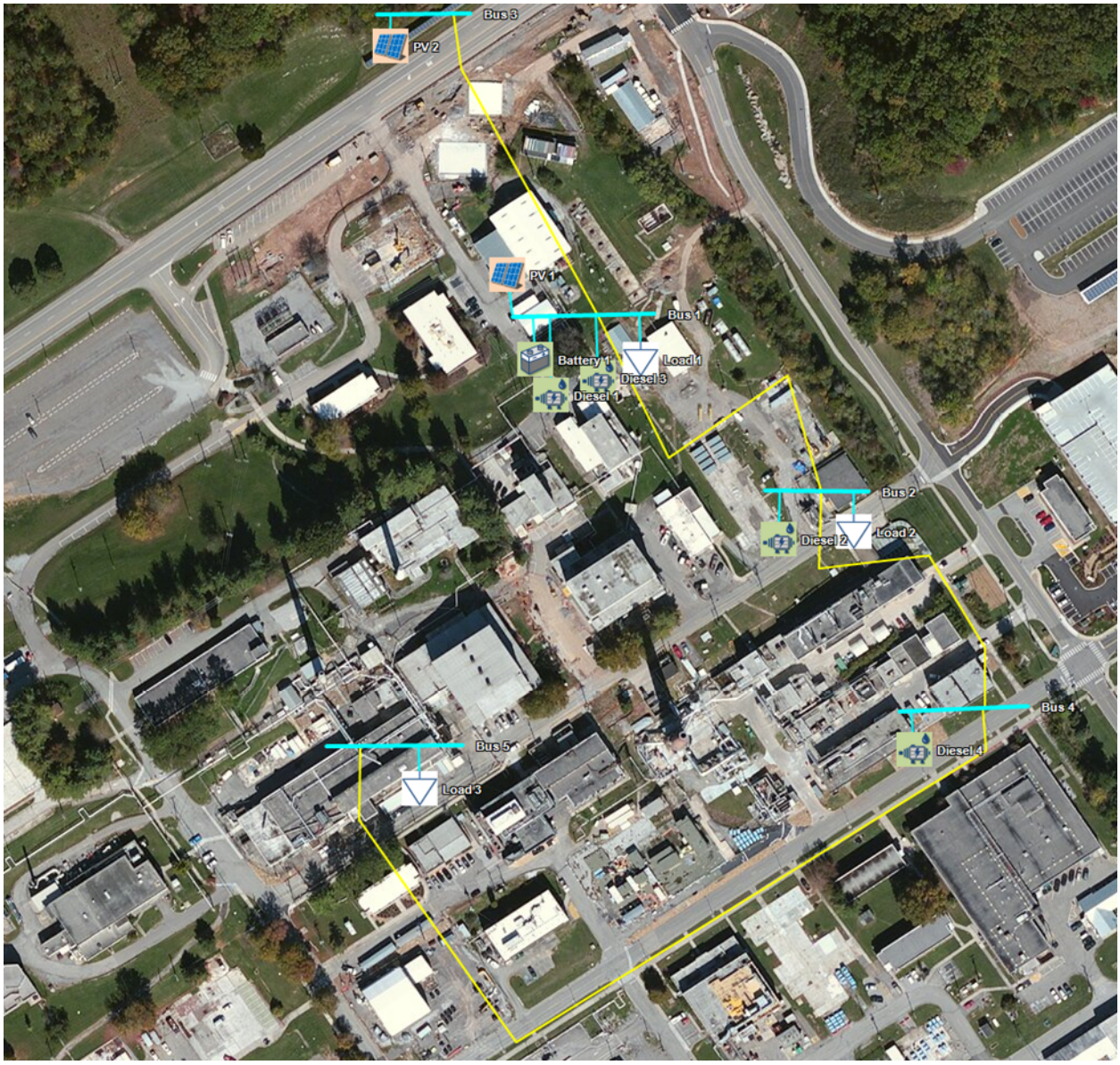

Figure 3. Modified ORNL DECC microgrid system.

Three multienergy loads are located on Bus 1, 2, and 5, respectively. The system peak electricity load is around 150 kW. The system peak heating load is around 100 kW, and the system peak cooling load is around 70 kW. The daily load profiles of the three multienergy loads are shown in Figure 4.

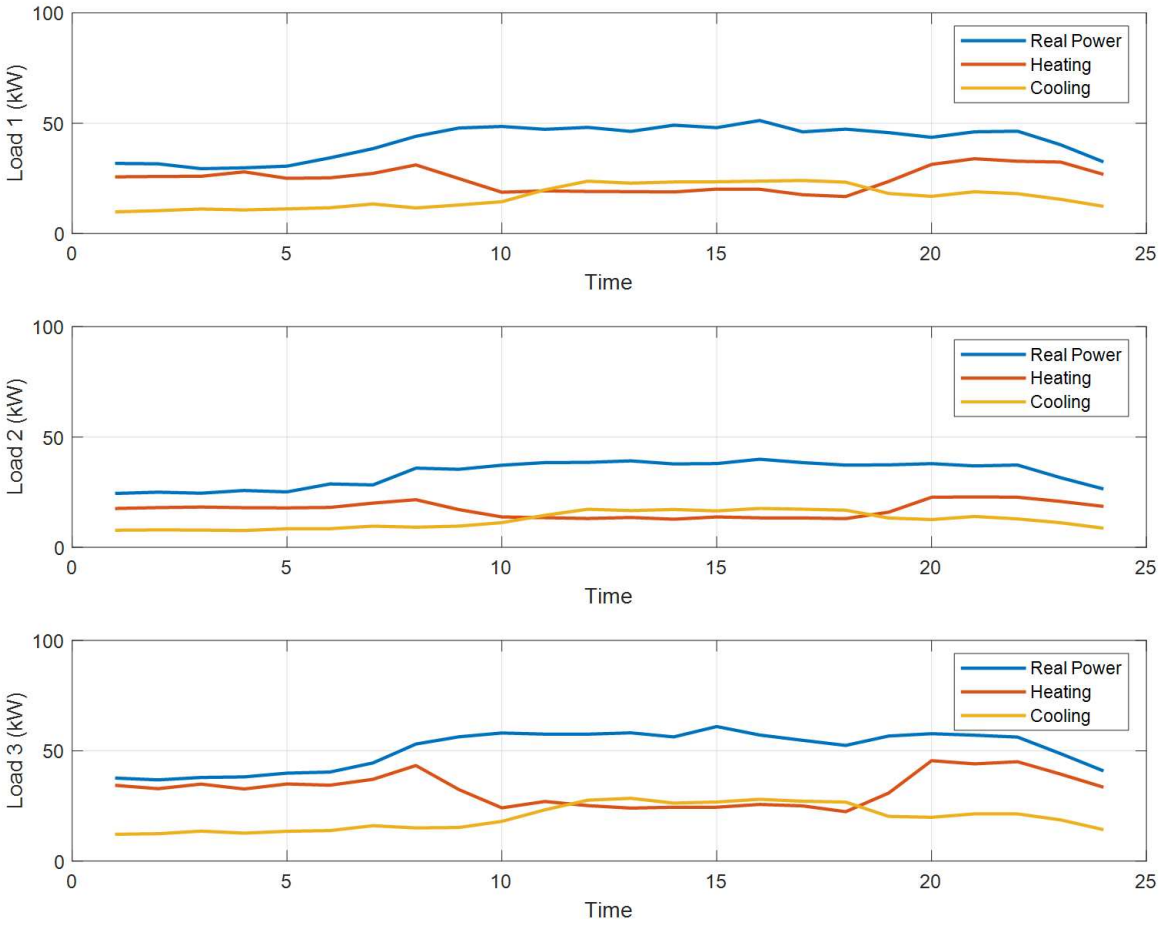

Figure 4. Multi-energy demand profiles.

There are two PV investment options: PV ground and PV roof. The initial capacity costs are 2548 and 2275 $/kW, separately. Both of them have life expectancy of 25 years. The parameters of the gas turbine and fuel cell investment options are listed in Table 2. The parameters of the gas turbine CHP and fuel cell CHP investment options are listed in Table 3. The parameters of the ESS investment options are listed in Table 4.

Table 2. Parameters of gas turbine and fuel cell investment options.

Technology	Capacity (kW)	Initial Capital Cost ($/kW)	O&M Cost ($/kW)	Minimum Output (kW)	Life Expectancy (Years)	No. of Candidate Units
Gas Turbine	125	660	0.013	37.5	20	5
	130	846	0.013	38.4	20	5
	760	900	0.013	228.6	20	5
Fuel Cell	210	6900	0.025	61	3	5
	262	6900	0.025	78.6	3	5

Table 3. Parameters of gas turbine CHP and fuel cell CHP investment options.

Technology	Capacity (kW)	Initial Capital Cost ($/kW)	O&M Cost ($/kW)	Minimum Power Output (kW)	Heat to Power Ratio	Life Expectancy (Years)	No. of Candidate Units
Gas Turbine CHP	5	5185	0.013	1.5	2.00	20	5
	35	1814	0.013	10.5	1.71	20	5
	65	3840	0.013	19.5	1.72	10	5
	130	1846	0.013	38.4	1.67	10	5
	760	1440	0.013	228.6	0.54	20	5
Fuel Cell CHP	300	3500	0.025	90	0.47	5	5
	440	4500	0.025	132	0.51	5	5
	1400	3900	0.025	420	0.46	5	5
	2800	4000	0.025	900	0.46	5	5

Table 4. Parameters of the ESS investment options.

Rated Energy (kWh)	Rated Power (kW)	Initial Capital Cost ($)	O&M Cost ($/year)	Minimum SOC (%)	Maximum SOC (%)	Round Trip Efficiency (%)	Life Expectancy (Years)	No. of Candidate Units
6.4	3.3	2730	1	25	95	0.92	10	5
30	15	21,000	120	25	95	0.94	10	5
70	30	191,730	5750	25	95	0.64	20	5
100	30	273,900	8220	25	95	0.64	20	5
400	200	800,100	24,000	25	95	0.65	20	5

Other constraint limits used in the case studies are listed in Table 5. Note that the number of energy blocks offered by DGs is assumed 3, i.e., $NI = 3$.

Table 5. Constraint limits used in the case studies.

Constraint	Minimum Value	Maximum Value
Invested PV Capacity (kW)	0	1000
Bus Voltage (p.u.)	0.95	1.05
Feeder Power Flow (kW)	−1500	1500
Power Factor of Gas turbine and Fuel cell	−0.5	0.5
Power Factor of Gas turbine CHP and Fuel cell CHP	−0.5	0.5
Power Factor of ESS	−0.5	0.5
Scheduled Power of m-th Block of Energy Offer by DGs	0	$\frac{P^{max} - P^{min}}{NI}$

Bus 1 voltage is set as 1.02 p.u. The analysis is conducted for a year with hourly time intervals. Each month is simplified as one day. So, only 12 days are considered in the optimization. The optimization model is programmed in MATLAB and solved by CPLEX 12.6 [59]. With a duality gap of 1%, the solution time of one case scatters from several minutes to several hours on a 2.66 GHz Windows-based PC with 4 GB of RAM.

3.2. Results of Case Studies

To test proposed model for microgrid expansion planning and operation, the following five cases have been studied using the modified ORNL DECC microgrid test system.

- Case 0: No investment available;
- Case 1: Only ESS investment available on bus 5;
- Case 2: Only ESS and PV investment available on bus 5;
- Case 3: All technology investment available on bus 5;
- Case 4: All technology investment available on all buses.

The optimized results for these five cases are compared in Table 6. Case 0 is the base case, which is basically the current microgrid system without any new investments. As can be seen in Table 6, the objective function of case 1 has the highest value. In addition, case 0 has the highest annualized total cost (investment cost and operating cost), the highest line power loss and the highest voltage deviations. In case 1, by investing 4 ESSs at bus 5, the annualized total cost (investment cost and operating cost) can be reduced by 10.3%. In addition, the loss and voltage deviations are also reduced significantly. In case 2, by investing another 145 kW PV at bus 5, the annualized total cost could be reduced by 19.5% compared to that of case 0. In case 3, by investing additional 35 kW gas turbine CHP at bus 5, the annualized total cost can be further reduced. With all kinds of technology investment available on all buses, the annualized cost can be reduced by 34.8% compared to that of case 0. This indicates that the siting of new components has significant impacts on the annualized total cost, the line power loss and the voltage deviations.

Table 6. Comparing optimization results of five cases.

Case No.	0	1	2	3	4
Objective Function	390,235	340,007	308,415	282,069	243,419
Investment Cost ($)	0	6146	29,148	33,039	53,526
Operating Cost ($)	361,295	317,900	261,579	235,107	181,856
Cost Reduction (%)	N/A	10.3	19.5	25.8	34.8
Line Power Loss (kWh)	28,524	15,801	17,427	13,535	7639
Voltage Deviation (p.u.)	416.6	160.2	260.4	387.7	197.9
New Investments	N/A	Two 3.3 kW/6.4 kWh ESSs; two 15 kW/30 kWh ESSs	Two 3.3 kW/6.4 kWh ESSs; two 15 kW/30 kWh ESSs; 146 kW PV roof	Two 3.3 kW/6.4 kWh ESSs; two 15 kW/30 kWh ESSs; 135 kW PV roof; one 35 kW gas turbine CHP	Bus 2 : Two 3.3 kW/6.4 kWh ESSs + Two 15 kW/30 kWh ESSs + One 35 kW gas turbine CHP+ 130 kW PV roof; Bus 5 : Two 3.3 kW/6.4 kWh ESSs + two 15 kW/30 kWh ESSs + one 35 kW gas turbine CHP + 64 kW PV roof

The total objective value, investment and operating costs, total line losses, and total voltage deviations among different cases are compared in Figure 5. As the case number increases, i.e., more investment options are enabled for the optimization, the total objective value decreases obviously. Theoretically, enabling more investment options means enlarging the feasible region. Therefore, the total objective value is reduced. As the investment cost increases, the operating cost decreases. Nevertheless, the annualized total cost (investment cost and operating cost together) strictly decreases, i.e., by investing new DGs and ESSs in an existing microgrid, the annualized overall cost of the microgrid could be reduced.

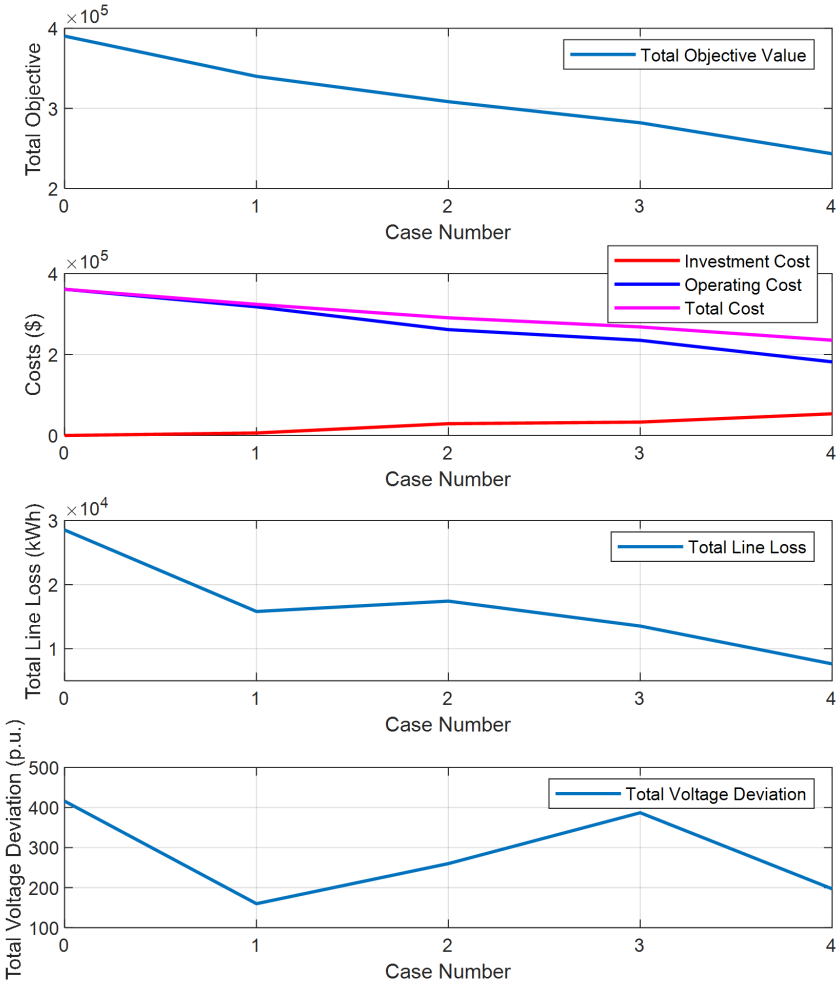

Figure 5. Comparison of total objective value, costs, losses, and total voltage deviations among different cases.

Beside costs, the total line losses and total voltage deviation are also included in the objective function as performance indices, which are compared in Figure 5. It should also be noted that the line power loss and voltage deviation are not always getting reduced as more investment options are enabled. This is because we are targeted to minimize the weighted multiobjective function, not individual objective. Meanwhile, the annualized total cost is dominating the total objective value, which could be seen from Table 6. In case 2 and 3, the total voltage deviation is sacrificed to get better weighted multiobjective function value.

To compare the voltage profiles of the system in different cases, the distribution density of bus voltages corresponding to all buses for the whole optimization horizon is shown in Figure 6. In particular, Figure 6a corresponds to the base case 0 in Table 6. As can been seen, the initial system has some low voltage issues. With new ESSs invested on bus 5 in case 1, the low voltage issues have been eliminated in Figure 6b. With additional PV invested on bus 5 in case 2, some high voltage issue starts to happen in Figure 6c. The high voltage issue is more obvious in Figure 6d when addition gas turbine CHP is installed on bus 5. This is due to the constraint that new investment options are only available on bus 5, which is at the end of the feeder. The voltage deviation is sacrificed for lower annualized total cost, so that the value of the objective function could be reduced as mentioned earlier. Relaxing this constraint and allowing all kinds of new investment options on all buses as in case 5, the high voltage issue is solved in Figure 6e by installing new ESSs, PV and gas

turbine CHP on bus 2, which is in the middle of the feeder. Alternatively, this issue could also be avoided by simply increasing the weighting factor of voltage deviation.

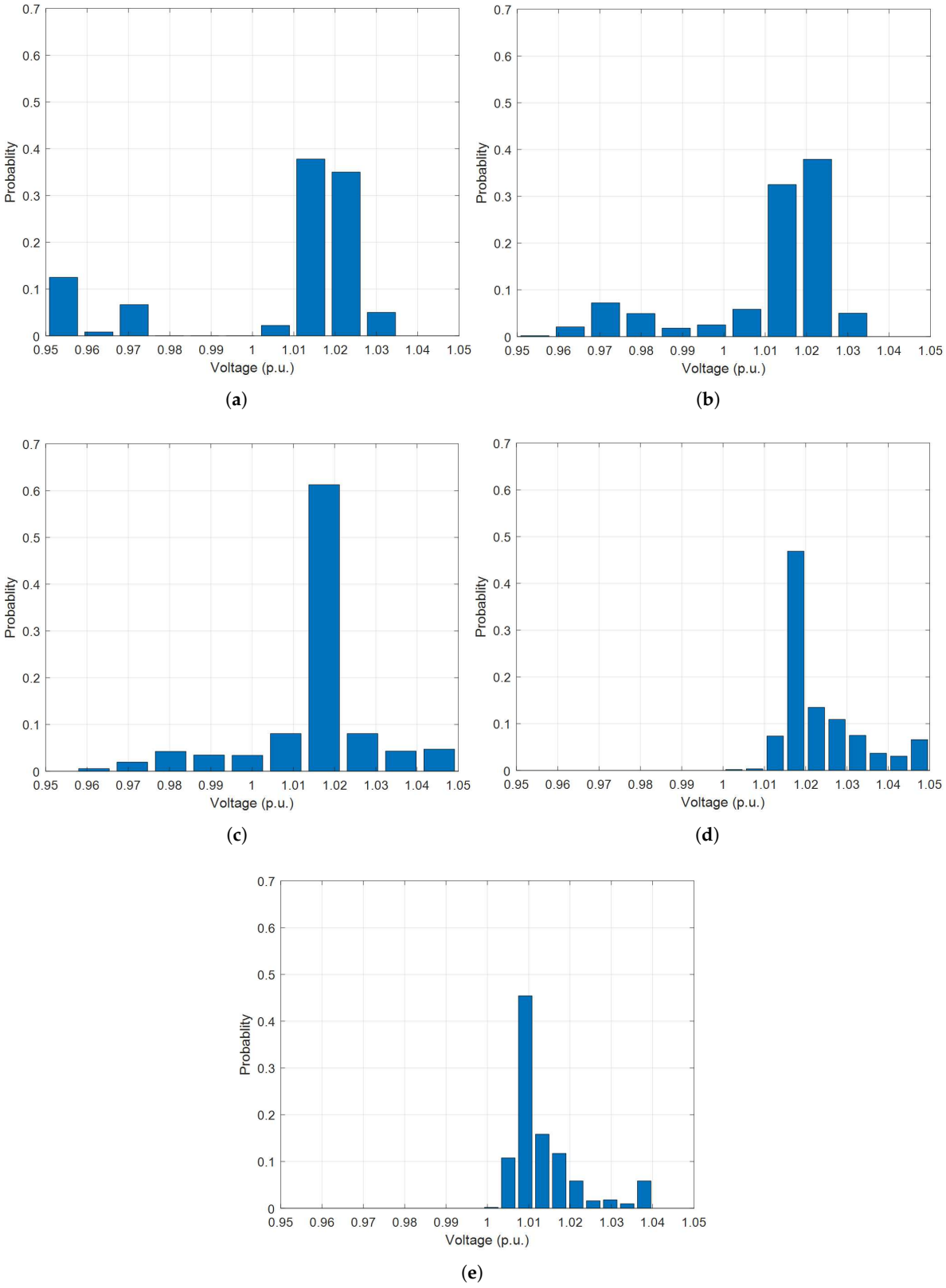

Figure 6. Distribution density of voltages for all nodes in different cases. (**a**) Case 0; (**b**) Case 1; (**c**) Case 2; (**d**) Case 3; (**e**) Case 4.

3.3. Sensitivity Analysis

To further validate the effectiveness of the proposed optimization model for optimal expansion planning and operation of remote microgrids, sensitivity analysis has been performed in this subsection. The sensitivity analysis is based on Case 2. In specific, the PV investment cost and ESS investment cost are multiplied by different scaling factors. Then, the invested PV capacity and ESS capacity under different investment costs are compared in Figure 7. When the PV investment cost is scaled from 0.5 to 1.5, the invested PV capacity increases from 127 kW to 162 kW, i.e., the higher cost of PV, the less invested PV capacity. Similarly, the invested ESS capacity decreases from 200 kWh to 42.8 kWh when the ESS investment cost is scaled from 0.5 to 1.5, i.e., the higher cost of ESS, the less invested ESS capacity.

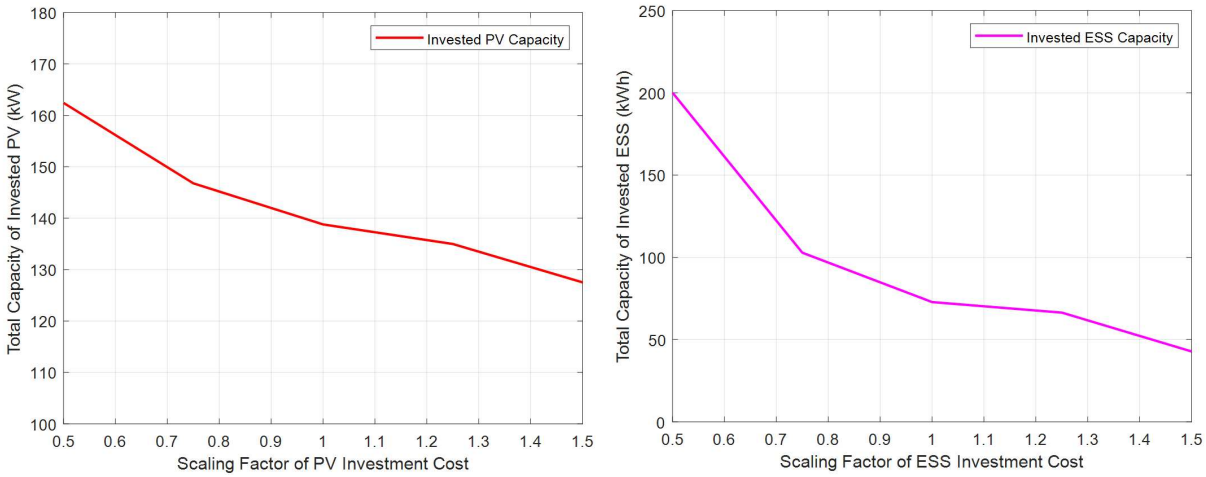

(**a**) (**b**)

Figure 7. Invested PV and ESS capacity under various scaling factors of PV and ESS investment cost. (**a**) Invested PV capacity under various PV investment cost; (**b**) Invested ESS capacity under various ESS investment cost.

4. Conclusions

In this paper, a three-stage MILP optimization is proposed for the optimal expansion planning and operation of remote microgrids. Considering various demands of electricity, heating, and cooling, the proposed MILP optimization minimizes the annualized costs of microgrids; meanwhile, enhance the performance of the system by determining the optimal DGs and ESSs mix selection, siting, sizing, and scheduling. For practical purpose, the available capacities of DGs and ESSs are modeled as discrete constants instead of continuous variables, and linearized power flow and heat flow equations are employed in the proposed model.

The proposed optimization model is validated by numerical simulation results on a remote microgrid consisting of DGs, ESSs, and various loads. Comparing with the base case, i.e., existing system without any investment, it has been shown that the annualized total cost could be significantly reduced (up to around 35%), by investing new DGs and ESSs on certain buses. Meanwhile, the total line losses and voltage deviation could be reduced, i.e., the system performance could be improved.

Future works to improve the proposed multienergy microgrid planning model include the following aspects:

- Expanding the current balanced power flow model to practical three-phase unbalanced situation.
- Improving the heat flow model to consider the heating losses of the heat distribution network.

- Enhancing the resilience of power supply under extreme weather events by integrating the reliability and resilience of microgrids into the objective function or constraints.

Author Contributions: G.L. carried out the main research tasks and wrote the full manuscript. Z.L. and Y.X. contributed to the development of the proposed methodology and the literature review. K.T. provided important suggestions on writing of the paper. All authors have read and agreed to the published version of the manuscript.

Funding: This research was funded by the U.S. Department of Energy's Office of Electricity Delivery and Energy Reliability (OE) under DOE/NETL project # M615000481. This work also made use of Engineering Research Center Shared Facilities supported by the Engineering Research Center Program of the National Science Foundation and the Department of Energy under NSF Award Number EEC-1041877 and the CURENT Industry Partnership Program.

Institutional Review Board Statement: Not applicable.

Informed Consent Statement: Not applicable.

Data Availability Statement: Not applicable.

Acknowledgments: This manuscript has been authored by UT-Battelle, LLC under Contract No. DE-AC05-00OR22725 with the U.S. Department of Energy. The United States Government retains and the publisher, by accepting the article for publication, acknowledges that the United States Government retains a non-exclusive, paid-up, published form of this manuscript, or allow others to do so, for United States Government purposes. The Department of Energy will provide public access to these results of federally sponsored research in accordance with the DOE Public Access Plan (http://energy.gov/downloads/doe-public-access-plan accessed on 1 March 2022).

Conflicts of Interest: The authors declare no conflict of interest.

Nomenclature

The symbols used in this paper are defined below. A bold symbol stands for its corresponding vector/matrix:

Indices and Numbers

n	Index of buses, running from 1 to NN
j	Index of selections for each technology
i	Index of numbers for a specific selection for each technology
t	Index of time periods, running from 1 to NT
m	Index of energy blocks offered by DGs, running from 1 to NI
NPV, NPV_{EX}	Number of photovoltaics (PV) investment selections and existing PV
NFC, NFC_{EX}	Number of fuel cell investment selections and existing fuel cells
NFC_j	Number of candidate units in fuel cell investment selection j
$NFCC$, $NFCC_{EX}$	Number of fuel cell combined heat and power (CHP) investment selections and existing fuel cell CHP
$NFCC_j$	Number of candidate units in fuel cell CHP investment selection j
NGT, NGT_{EX}	Number of gas turbine investment selections and existing gas turbines
NGT_j	Number of candidate units in gas turbine investment selection j
$NGTC$, $NGTC_{EX}$	Number of gas turbine CHP investment selections and existing gas turbine CHP
$NGTC_j$	Number of candidate units in gas turbine CHP investment selection j
NBT, NBT_{EX}	Number of energy storage system (ESS) investment selections and existing ESSs
NBT_j	Number of candidate units in ESS investment selection j

Variables

Binary Variables

U_{nji}^{FC}	1 if fuel cell i of size selection j is invested at bus n and 0 otherwise.
U_{nji}^{FCC}	1 if fuel cell CHP i of size selection j is invested at bus n and 0 otherwise.
U_{nji}^{GT}	1 if gas turbine i of size selection j is invested at bus n and 0 otherwise.

U_{nji}^{GTC}	1 if gas turbine CHP i of size selection j is invested at bus n and 0 otherwise.
U_{nji}^{BT}	1 if ESS i of size selection j is invested at bus n and 0 otherwise.
u_{njit}^{FC}	1 if fuel cell i of size selection j at bus n is scheduled on during period t and 0 otherwise.
u_{njit}^{FCC}	1 if fuel cell CHP i of size selection j at bus n is scheduled on during period t and 0 otherwise.
u_{njit}^{GT}	1 if gas turbine i of size selection j at bus n is scheduled on during period t and 0 otherwise.
u_{njit}^{GTC}	1 if gas turbine CHP i of size selection j at bus n is scheduled on during period t and 0 otherwise.
u_{njit}^{C}, u_{njit}^{D}	1 if ESS i of size selection j at bus n is scheduled charging/discharging during time t and 0 otherwise.
$u_{it}^{FC_{EX}}$	1 if existing fuel cell i is scheduled on during period t and 0 otherwise.
$u_{it}^{FCC_{EX}}$	1 if existing fuel cell CHP i is scheduled on during period t and 0 otherwise.
$u_{it}^{GT_{EX}}$	1 if existing gas turbine i is scheduled on during period t and 0 otherwise.
$u_{it}^{GTC_{EX}}$	1 if existing gas turbine CHP i is scheduled on during period t and 0 otherwise.
$u_{it}^{DG_{EX}}$	1 if existing diesel generator i is scheduled on during period t and 0 otherwise.
Continuous Variables	
Cap_{ni}^{PV}	Invested capacity of PV selection i at bus n.
P_{nit}^{PV}	Power of invested PV selection i at bus n during period t.
$p_{njit}^{FC}(m)$	Power output scheduled from the m-th block of energy offer by fuel cell i of size selection j at bus n during period t. Limited to $p_{njit}^{FC,\max}(m)$.
$p_{njit}^{FCC}(m)$	Power output scheduled from the m-th block of energy offer by fuel cell CHP i of size selection j at bus n during period t. Limited to $p_{njit}^{FCC,\max}(m)$.
$p_{njit}^{GT}(m)$	Power output scheduled from the m-th block of energy offer by gas turbine i of size selection j at bus n during period t. Limited to $p_{njit}^{GT,\max}(m)$.
$p_{njit}^{GTC}(m)$	Power output scheduled from the m-th block of energy offer by gas turbine CHP i of size selection j at bus n during period t. Limited to $p_{njit}^{GTC,\max}(m)$.
p_{njit}^{ch}, p_{njit}^{dch}	Charging/discharging power of ESS i of size selection j at bus n during period t. Limited to $P_{j}^{ch,\max}$ and $P_{j}^{dch,\max}$.
G_{nt}	Purchased natural gas for direct heating at bus n during time t.
P_{ft}, Q_{ft}	Real/ reactive power on line f during period t.
P_{njit}^{FC}, Q_{njit}^{FC}	Real/reactive power output of fuel cell i of size selection j at bus n during period t.
P_{njit}^{FCC}, Q_{njit}^{FCC}	Real/reactive power output of fuel cell CHP i of size selection j at bus n during period t.
P_{njit}^{GT}, Q_{njit}^{GT}	Real/reactive power output of gas turbine i of size selection j at bus n during period t.
P_{njit}^{GTC}, Q_{njit}^{GTC}	Real/reactive power output of gas turbine CHP i of size selection j at bus n during period t.
Q_{njit}^{BT}	Reactive power output of ESS i of size selection j at bus n during period t.
SOC_{njit}	State of charge of ESS i of size selection j at bus n during period t.
V_{nt}	Voltage magnitude of bus n during period t.
H_{njit}^{FCC}	Heating power output of fuel cell CHP i of size selection j at bus n during period t.
H_{njit}^{GTC}	Heating power output of gas turbine CHP i of size selection j at bus n during period t.

H_{nt}^{H}, H_{nt}^{C} Heating power serving heating/cooling demand at bus n during time t.
P_{nt}^{H}, P_{nt}^{C} Heat pump power consumption for heating/cooling demand at bus n during time t.
X_{nt}^{V} Auxiliary variables

Constants

$\lambda_j^{FC}(m)$ Marginal cost of the m-th block of energy offer by fuel cell selection j.
$\lambda_j^{FCC}(m)$ Marginal cost of the m-th block of energy offer by fuel cell CHP selection j.
$\lambda_j^{GT}(m)$ Marginal cost of the m-th block of energy offer by gas turbine selection j.
$\lambda_j^{GTC}(m)$ Marginal cost of the m-th block of energy offer by gas turbine CHP selection j.
$\lambda_j^{ch}(m)$, $\lambda_j^{dch}(m)$ Charging/discharging cost ESS selection j.
λ_{nt}^{G} Natural gas price at bus n during period t.
r Annual interest rate. Set as 5%.
l_i^{PV}, l_j^{BT} Lifetime of PV/ESS selection i.
l_j^{FC}, l_j^{FCC} Lifetime of fuel cell/fuel cell CHP selection j.
l_j^{GT}, l_j^{GTC} Lifetime of gas turbine/gas turbine CHP selection j.
C_i^{PV}, C_j^{BT} Initial investment cost of PV/ESS selection i.
C_j^{FC}, C_j^{FCC} Initial investment cost of fuel cell/fuel cell CHP selection j.
C_j^{GT}, C_j^{GTC} Initial investment cost of gas turbine/gas turbine CHP selection j.
Cap_j^{FC}, Cap_j^{FCC} Rated capacity of fuel cell/fuel cell CHP selection j.
Cap_j^{GT}, Cap_j^{GTC} Rated capacity of gas turbine/gas turbine CHP selection j.
COM_i^{PV} Operation & Maintenance (O&M) cost of PV selection i.
COM_j^{FC}, COM_j^{FCC} O&M cost of fuel cell/fuel cell CHP selection j.
COM_j^{GT}, COM_j^{GTC} O&M cost of gas turbine/gas turbine CHP selection j.
COM_j^{BT} O&M cost of ESS selection j.
κ_j^{FC} Operating Cost of fuel cell selection j at the point of $P_j^{FC,\min}$.
κ_j^{FCC} Operating Cost of fuel cell CHP selection j at the point of $P_j^{FCC,\min}$.
κ_j^{GT} Operating Cost of gas turbine selection j at the point of $P_j^{GT,\min}$.
κ_j^{GTC} Operating Cost of gas turbine CHP selection j at the point of $P_j^{GTC,\min}$.
$V_{\text{thr}}^{\max}$, $V_{\text{thr}}^{\min}$ Maximum/Minimum voltage thresholds beyond which voltage deviation will be minimized.
$V^{\max}$, $V^{\min}$ Maximum/Minimum voltage deviations.
r_f, x_f Resistance and reactance of line f.
S_i^{PV} Size of unit capacity of PV selection i.
Δ_n^{max} Maximum area for PV investment at bus n.
$P_j^{\text{FC,max}}$, $P_j^{\text{FC,min}}$ Maximum/minimum power of fuel cell selection j.
$P_j^{\text{FCC,max}}$, $P_j^{\text{FCC,min}}$ Maximum/minimum power of fuel cell CHP selection j.
$P_j^{\text{GT,max}}$, $P_j^{\text{GT,min}}$ Maximum/minimum power of gas turbine selection j.
$P_j^{\text{GTC,max}}$, $P_j^{\text{GTC,min}}$ Maximum/minimum power of gas turbine CHP selection j.
$SOC_j^{\text{BT,max}}$, $SOC_j^{\text{BT,min}}$ Maximum/minimum state of charge of ESS selection j.
η_j^{C}, η_j^{D} ESS selection j charging/discharging efficiency factor.
$PF_j^{FC,min}$, $PF_j^{FC,max}$ Power factor limit of fuel cell selection j.
$PF_j^{FCC,min}$, $PF_j^{FCC,max}$ Power factor limit of fuel cell CHP selection j.
$PF_j^{GT,min}$, $PF_j^{GT,max}$ Power factor limit of gas turbine selection j.
$PF_j^{GTC,min}$, $PF_j^{GTC,max}$ Power factor limit of gas turbine CHP selection j.
$PF_j^{BT,C,min}$, $PF_j^{BT,C,max}$ Power factor limit of ESS selection j when charging.
$PF_j^{BT,D,min}$, $PF_j^{BT,D,max}$ Power factor limit of ESS selection j when discharging.
S_j^{FC}, S_j^{FCC} Apparent power limit of fuel cell/fuel cell CHP selection j.
S_j^{GT}, S_j^{GTC} Apparent power limit of gas turbine/gas turbine CHP selection j.
S_j^{BT} Apparent power limit of ESS selection j.
S_f Apparent power limit of line f.

HPR_j^{FCC}	Heat to power ratio of fuel cell CHP selection j.
HPR_j^{GTC}	Heat to power ratio of gas turbine CHP selection j.
L_{nt}^H, L_{nt}^C	Heating/cooling demand at bus n during time t.
β^R	Heat recovery efficiency of CHP generators
β^G	Efficiency of burning natural gas for heating.
δ^H, δ^C	Coefficient of performance (COP) of heat pump for heating/cooling.
γ^C	COP of absorption chiller.

References

1. Cagnano, A.; De Tuglie, E.; Mancarella, P. Microgrids: Overview and guidelines for practical implementations and operation. *Appl. Energy* **2020**, *258*, 114039 [CrossRef]
2. Khan, M.Z.; Mu, C.; Habib, S.; Alhosaini, W.; Ahmed, E.M. An Enhanced Distributed Voltage Regulation Scheme for Radial Feeder in Islanded Microgrid. *Energies* **2021**, *14*, 6092. [CrossRef]
3. Park, B.; Zhang, Y.; Olama, M.; Kuruganti, T. Model-free control for frequency response support inmicrogrids utilizing wind turbines. *Electr. Power Syst. Res.* **2021**, *194*, 107080 [CrossRef]
4. Liu, R.; Wang, S.; Liu, G.; Wen, S.; Zhang, J.; Ma, Y. An Improved Virtual Inertia Control Strategy for Low Voltage AC Microgrids with Hybrid Energy Storage Systems. *Energies* **2022**, *15*, 442. [CrossRef]
5. Wang, Y.; Rousis, A.O.; Strbac, G. On microgrids and resilience: A comprehensive review on modeling and operational strategies. *Renew. Sustain. Energy Rev.* **2020**, *134*, 110313. [CrossRef]
6. Warneryd, M.; Hakansson, M.; Karltorp, K. Unpacking the complexity of community microgrids: A review of institutions′ roles for development of microgrids. *Renew. Sustain. Energy Rev.* **2020**, *121*, 109690. [CrossRef]
7. Guidehouse Insights Report. Microgrid Deployment Tracker 1Q20. 2020. Available online: https://guidehouseinsights.com/reports/determining-the-top-10-countries-for-microgrid-projects-and-total-installed-capacity (accessed on 1 March 2022).
8. Gamarra, C.; Guerrero, J.M. Computational optimization techniques applied to microgrids planning: A review. *Renew. Sustain. Energy Rev.* **2015**, *48*, 413–424. [CrossRef]
9. Khezri, R.; Mahmoudi, A.; Aki, H.; Muyeen, S.M. Optimal Planning of Remote Area Electricity Supply Systems: Comprehensive Review, Recent Developments and Future Scopes. *Energies* **2021**, *14*, 5900. [CrossRef]
10. Vafaei, M.; Kazerani, M. Optimal unit-sizing of a wind-hydrogen-diesel microgrid system for a remote community. In Proceedings of the 2011 IEEE Trondheim PowerTech, Trondheim, Norway, 19–23 June 2011; pp. 1–7.
11. Hajipour, E.; Bozorg, M.; Fotuhi-Firuzabad, M. Stochastic Capacity Expansion Planning of Remote Microgrids with Wind Farms and Energy Storage. *IEEE Trans. Sustain. Energy* **2015**, *6*, 491–498. [CrossRef]
12. Alharbi, H.; Bhattacharya, K. Stochastic Optimal Planning of Battery Energy Storage Systems for Isolated Microgrids. *IEEE Trans. Sustain. Energy* **2018**, *9*, 211–227. [CrossRef]
13. Jithendranath, J.; Das, D. Stochastic planning of islanded microgrids with uncertain multi-energy demands and renewable generations. *IET Renew. Power Gener.* **2020**, *14*, 4179–4192. [CrossRef]
14. Yu, J.; Ryu, J.H.; Lee, I.B. A stochastic optimization approach to the design and operation planning of a hybrid renewable energy system. *Appl. Energy* **2019**, *247*, 212–220. [CrossRef]
15. Narayan, A.; Ponnambalam, K. Risk-averse stochastic programming approach for microgrid planning under uncertainty. *Renew. Energy* **2017**, *101*, 399–408. [CrossRef]
16. Hakimi, S.M.; Hasankhani, A.; Shafie-khah, M.; Catalao, J.P. Stochastic planning of a multi-microgrid considering integration of renewable energy resources and real-time electricity market. *Appl. Energy* **2021**, *298*, 117215. [CrossRef]
17. Alonso, A.; de la Hoz, J.; Martin, H.; Coronas, S.; Salas, P.; Matas, J. A Comprehensive Model for the Design of a Microgrid under Regulatory Constraints Using Synthetical Data Generation and Stochastic Optimization. *Energies* **2020**, *13*, 5590. [CrossRef]
18. Khayatian, A.; Barati, M.; Lim, G.J. Integrated Microgrid Expansion Planning in Electricity Market with Uncertainty. *IEEE Trans. Power Syst.* **2018**, *33*, 3634–3643. [CrossRef]
19. Wu, D.; Ma, X.; Huang, S.; Fu, T.; Balducci, P. Stochastic optimal sizing of distributed energy resources for a cost-effective and resilient Microgrid. *Energy* **2020**, *198*, 117284. [CrossRef]
20. Wang, Z.; Chen, B.; Wang, J.; Kim, J.; Begovic, M. Robust Optimization Based Optimal DG Placement in Microgrids. *IEEE Trans. Smart Grid* **2014**, *5*, 2173–2182. [CrossRef]
21. Khodaei, A. Provisional Microgrid Planning. *IEEE Trans. Smart Grid* **2017**, *8*, 1096–1104. [CrossRef]
22. Dehghan, A.; Nakiganda, A.; Aristidou, P. A Data-Driven Two-Stage Distributionally Robust Planning Tool for Sustainable Microgrids. In Proceedings of the IEEE Power & Energy Society General Meeting (PESGM), Virtual, 3–6 August 2020; pp. 1–5.
23. Nakiganda, A.M.; Dehghan, S.; Markovic, U.; Hug, G.; Aristidou, P. A Stochastic-Robust Approach for Resilient Microgrid Investment Planning Under Static and Transient Islanding Security Constraints. *IEEE Trans. Smart Grid* **2022**. [CrossRef]
24. Babaei, R.; Ting, D.; Carriveau, R. Feasibility and optimal sizing analysis of stand-alone hybrid energy systems coupled with various battery technologies: A case study of Pelee Island. *Energy Rep.* **2022**, *8*, 4747–4762. [CrossRef]
25. Heleno M.; Ren, Z. Multi-Energy Microgrid Planning Considering Heat Flow Dynamics. *IEEE Trans. Energy Convers.* **2021**, *36*, 1962–1971. [CrossRef]

26. Kaab, A.; Sharifi, M.; Mobli, H.; Nabavi-Pelesaraei, A.; Chau, K.W. Use of optimization techniques for energy use efficiency and environmental life cycle assessment modification in sugarcane production. *Energy* **2019**, *181*, 1298–1320. [CrossRef]
27. Acevedo-Arenas, C.Y.; Correcher, A.; Sanchez-Diaz, C.; Ariza, E.; Alfonso-Solar, D.; Vargas-Salgado, C.; Petit-Suarez, J.F. MPC for optimal dispatch of an AC-linked hybrid PV/wind/biomass/H2 system incorporating demand response. *Energy Convers. Manag.* **2019**, *186*, 241–257. [CrossRef]
28. Combe, M.; Mahmoudi, A.; Haque, M.H.; Khezri, R. AC-coupled hybrid power system optimisation for an Australian remote community. *Int. Trans. Electr. Energy Syst.* **2020**, *30*, 12503. [CrossRef]
29. Prathapaneni, D.R.; Detroja, K.P. An integrated framework for optimal planning and operation schedule of microgrid under uncertainty. *Sustain. Energy Grids Netw.* **2019**, *19*, 100232. [CrossRef]
30. Katsigiannis, Y.A.; Georgilakis, P.S.; Karapidakis, E.S. Hybrid simulated annealing–tabu search method for optimal sizing of autonomous power systems with renewables. *IEEE Trans. Sustain. Energy* **2012**, *3*, 330–338. [CrossRef]
31. Lu, X.; Wang, H. Optimal Sizing and Energy Management for Cost-Effective PEV Hybrid Energy Storage Systems. *IEEE Trans. Ind. Inform.* **2020**, *16*, 3407–3416. [CrossRef]
32. Askarzadeh, A. Distribution generation by photovoltaic and diesel generator systems: Energy management and size optimization by a new approach for a stand-alone application. *Energy* **2017**, *122*, 542–551. [CrossRef]
33. Bukar, A.L.; Tan, C.W.; Lau, K.Y. Optimal sizing of an autonomous photovoltaic/wind/battery/diesel generator microgrid using grasshopper optimization algorithm. *Sol. Energy* **2019**, *188*, 685–696. [CrossRef]
34. El-Bidairi, K.S.; Nguyen, H.D.; Jayasinghe, S.D.; Mahmoud, T.S.; Penesis, I. Impact of tidal energy on battery sizing in standalone microgrids: A case study. In Proceedings of the 2018 IEEE International Conference on Environment and Electrical Engineering and 2018 IEEE Industrial and Commercial Power Systems Europe, Palermo, Italy, 12–15 June 2018; pp. 1–6.
35. Diab, A.A.Z.; Sultan, H.M.; Mohamed, I.S.; Kuznetsov, O.N.; Do, T.D. Application of Different Optimization Algorithms for Optimal Sizing of PV/Wind/Diesel/Battery Storage Stand-Alone Hybrid Microgrid. *IEEE Access* **2019**, *7*, 119223–119245. [CrossRef]
36. Shahid, F.; Zameer, A.; Muneeb, M. A novel genetic LSTM model for wind power forecast. *Energy* **2021**, *223*, 1200692. [CrossRef]
37. Mora, E.; Cifuentes, J.; Marulanda, G. Short-Term Forecasting of Wind Energy: A Comparison of Deep Learning Frameworks. *Energies* **2021**, *14*, 7943. [CrossRef]
38. Ahmed, R.; Sreeram, V.; Mishra, Y.; Arif, M.D. A review and evaluation of the state-of-the-art in PV solar power forecasting: Techniques and optimization. *Renew. Sust. Energ. Rev.* **2020**, *124*, 109792. [CrossRef]
39. Sundararajan, A.; Ollis, B. Regression and Generalized Additive Model to Enhance the Performance of Photovoltaic Power Ensemble Predictors. *IEEE Access* **2021**, *9*, 111899–111914. [CrossRef]
40. Liu, G.; Jiang, T.; Ollis, T.B.; Zhang, X.; Tomsovic, K. Distributed energy management for community microgrids considering network operational constraints and building thermal dynamics. *Appl. Energy* **2019**. *239*, 83–95. [CrossRef]
41. Carrion, M.; Arroyo, J.M. A computationally efficient mixed-integer linear formulation for the thermal unit commitment problem. *IEEE Trans. Power Syst.* **2006**, *21*, 1371–1378. [CrossRef]
42. Zhang, H.; Vittal, V.; Heydt, G.T.; Quintero, J. A mixed-integer linear programming approach for multi-stage security-constrained transmission expansion planning. *IEEE Trans. Power Syst.* **2012**, *27*, 1125–1133. [CrossRef]
43. Stadler, M.; Pecenak, Z.; Mathiesen, P.; Fahy, K.; Kleissl, J. Performance Comparison between Two Established Microgrid Planning MILP Methodologies Tested On 13 Microgrid Projects. *Energies* **2020**, *13*, 4460. [CrossRef]
44. Herrero, I.; Rodilla, P.; Batlle, C. Evolving Bidding Formats and Pricing Schemes in USA and Europe Day-Ahead Electricity Markets. *Energies* **2020**, *13*, 5020. [CrossRef]
45. Hogan, W. Electricity Market Design and Efficient Pricing: Applications for New England and Beyond. *Electr. J.* **2014**, *27*, 23–49. [CrossRef]
46. Zia, M.F.; Elbouchikhi, E.; Benbouzid, M. Optimal operational planning of scalable DC microgrid with demand response, islanding, and battery degradation cost considerations. *Appl. Energy* **2019**, *237*, 695–707. [CrossRef]
47. Li, Y.; Zhao, T.; Wang, P.; Gooi, H.; Wu, L.; Liu, Y.; Ye, J. Optimal Operation of Multimicrogrids via Cooperative Energy and Reserve Scheduling. *IEEE Trans. Ind. Inf.* **2018**, *14*, 3459–3468. [CrossRef]
48. Su, W.; Wang, J.; Roh, J. Stochastic energy scheduling in microgrids with intermittent renewable energy resources. *IEEE Trans. Smart Grid* **2014**, *5*, 1876–1883. [CrossRef]
49. Chen, S.; Gooi, H.B.; Wang, M. Sizing of Energy Storage for Microgrids. *IEEE Trans. Smart Grid* **2012**, *3*, 142–151. [CrossRef]
50. Baran, M.E.; Wu, F.F. Network reconfiguration in distribution systems for loss reduction and load balancing. *IEEE Trans. Power Deliv.* **1989**, *4*, 1401–1407. [CrossRef]
51. Marti, J.R.; Ahmadi, H.; Bashualdo, L. Linear power-flow formulation based on a voltage-dependent load mode. *IEEE Trans. Power Deliv.* **2013**, *28*, 1682–1690. [CrossRef]
52. Purchala, K.; Meeus, L.; Van Dommelen, D.; Belmans, R. Usefulness of DC power flow for active power flow analysis. In Proceedings of the IEEE Power Engineering Society General Meeting, San Francisco, CA, USA, 16 June 2005; pp. 454–459.
53. Xin, N.; Chen, L.; Ma, L.; Si, Y. A Rolling Horizon Optimization Framework for Resilient Restoration of Active Distribution Systems. *Energies* **2022**, *15*, 3090. [CrossRef]
54. Huang, J.; Cui, B.; Zhou, X.; Bernstein, A. A Generalized LinDistFlow Model for Power Flow Analysis. In Proceedings of the 2021 60th IEEE Conf. on Decision and Control (CDC), Austin, TX, USA, 13–17 December 2021; pp. 3493–3500.

55. Liu, G.; Starke, M.; Zhang, X.; Tomsovic, K. A MILP-based distribution optimal power flow model for microgrid operation. In Proceedings of the IEEE Power and Energy Society General Meeting (PESGM), Boston, MA, USA, 17–21 July 2016; pp. 1–5.
56. Xiao, B.; Starke, M.; Liu, G.; Ollis, B.; Irminger, P.; Dimitrovski, A.; Prabakar, K.; Dowling, K.; Xu, Y. Development of hardware-in-the-loop microgrid testbed. In Proceedings of the IEEE Energy Convers Congr Expo (ECCE), Montreal, QC, Canada, 20–24 September 2015; pp. 1196–1202.
57. Liu, G.; Xu, Y.; Tomsovic, K. Bidding Strategy for Microgrid in Day-Ahead Market Based on Hybrid Stochastic/Robust Optimization. *IEEE Trans. Smart Grid* **2016**, *7*, 227–237. [CrossRef]
58. Oak Ridge National Laboratory (ORNL) Rotating Shadowband Radiometer (RSR). Available online: https://www.nrel.gov/midc/ornl_rsr/ (accessed on 1 March 2022).
59. The IBM ILOG CPLEX Optimization Studio. 2022. Available online: https://www.ibm.com/products/ilog-cplex-optimization-studio?utm_content=SRCWW&p1=Search&p4=43700068101114289&p5=p&gclid=Cj0KCQjwpImTBhCmARIsAKr58cwVzPZygvnYZkYfM94KJmcGR7pC7Nmmu3dlF7NP3sgLvwIlsraxzNMaAihbEALw_wcB&gclsrc=aw.ds (accessed on 1 March 2022).